Photobiomodulation Inhibits the Activation of Neurotoxic Microglia and Astrocytes Through Inhibiting the Crosstalk of Lcn2/JAK2-STAT3 after Spinal Cord Injury in Rats

Xuankang Wang
Xijing Hospital Department of Orthopaedics
Xin Li
Xijing Hospital Department of Orthopaedics
Xiaoshuang Zuo
Xijing Hospital Department of Orthopaedics
Zhuowen Liang
Xijing Hospital Department of Orthopaedics
Zhe Wang (wangzhe@fmmu.edu.cn)
Xijing Hospital Institute of Orthopaedics: Xijing Hospital Department of Orthopaedics
Tan Ding
Xijing Hospital Department of Orthopaedics
Kun Li
Xijing Hospital Department of Orthopaedics
Yangguang Ma
Xijing Hospital Department of Orthopaedics
Penghui Li
Xijing Hospital Department of Orthopaedics
Zhijie Zhu
Xijing Hospital Department of Orthopaedics
Cheng Ju
Xijing Hospital Department of Orthopaedics
Zhihao Zhang
Xijing Hospital Department of Orthopaedics
Zhiwen Song
Xijing Hospital Department of Orthopaedics
Huilin Quan
Xijing Hospital Department of Orthopaedics
Jiawei Zhang
Xijing Hospital Department of Orthopaedics

Xueyu Hu
Xijing Hospital Department of Orthopaedics

Research

Keywords: Neuroinflammation, Spinal cord injury, M1 microglia, A1 astrocytes, Lcn2, JAK2-STAT3

Posted Date: May 7th, 2021

DOI: https://doi.org/10.21203/rs.3.rs-471722/v1

Abstract

Background

In situ microglia and astrocytes begin to activate and participate in neuroinflammation after spinal cord injury (SCI), and the high expression of lipocalin 2 (Lcn2) and the activation of the Janus kinase-2 (JAK2)-signal transducer and activator of transcription-3 (STAT3) pathway promote the polarization of activated microglia and astrocytes towards the neurotoxic phenotype (M1 microglia and A1 astrocytes). We previously reported that photobiomodulation (PBM) can promote functional recovery by reducing neuroinflammation after SCI, but the mechanism of PBM on the microglia and astrocytes involved is still unclear. Therefore, the purpose of this study was to explore the role of the Lcn2 and JAK2-STAT3 pathways in the activation of M1 and A1 and the mechanism by which PBM may play a therapeutic role.

Methods

PBM intervention was performed every day after the SCI model was established, and the activation of microglia and astrocytes was observed at different time points post injury (1, 3, 7, 14, 28 dpi). The level of tissue apoptosis, the number of surviving neurons, the recovery of motor function, the level of Lcn2 and the activation of JAK2-STAT3 were evaluated in the PBM group and the vehicle group. M1 and A1 cells were irradiated with PBM in vitro, and the JAK2-STAT3 pathway inhibitor cucurbitacin I, adenovirus transfection and recombinant Lcn2 protein were cotreated with PBM to explore the mechanism of the activation of M1 and A1 and the underlying effect of PBM.

Results

PBM inhibited the activation of neurotoxic microglia and astrocytes, decreased secondary inflammation and tissue apoptosis, increased the number of neurons retained, and promoted the recovery of motor function after SCI. The upregulation of Lcn2 and the activation of the JAK2-STAT3 pathway after SCI were suppressed by PBM. In vitro experiments also proved that PBM can inhibit the activation of M1 microglia and A1 astrocytes, and the effect is related to the level of Lcn2 and the activation of the JAK2-STAT3 pathway.

Conclusion

The crosstalk of Lcn2/JAK2-STAT3 is involved in the activation of neurotoxic microglia and astrocytes after SCI, and this process can be alleviated by PBM.

Introduction

According to reports, approximately 27 million people in the world have lost the ability to take care of themselves due to spinal cord injury (SCI) as of 2016, and the incidence of SCI has shown a significant increase worldwide in recent years[1]. Neuroinflammation in SCI is receiving increasing attention due to its complex and contradictory effects. It is initially a defence mechanism that removes cell debris and

promotes tissue repair[2], but continuous inflammation is harmful and may lead to failure of tissue repair. As innate immune cells in situ, microglia and astrocytes are ubiquitously distributed throughout the brain and spinal cord, playing an important role in pathology and repair[3]. According to their activation state under injury or pathological conditions, they can be divided into two distinct phenotypes: neurotoxic microglia and astrocytes (M1 type and A1 type) and neuroprotective microglia and astrocytes (M2 type and A2 type)[4]. M1-type microglia that express CD16/CD32, inducible nitric oxide synthase (iNOS) and other markers tend to release destructive mediators, including tumour necrosis factor-α (TNF-α), interleukin-1β (IL-1β) and interleukin-6 (IL-6)[5], which are harmful to tissue repair. A1 astrocytes with C3 as a marker have lost most of their normal functions, leading to abnormal synthesis and release of neurotransmitters, disrupting synapse formation, rapidly killing neurons and mature differentiated oligodendrocytes[6]. It should be emphasized that microglia and astrocytes are closely related, and they always respond as one unit when the central nervous system (CNS) is perturbed. A1 astrocytes activate the secretion of interleukin-1α (IL-1α), component 1q (C1q) and TNF-α by activated microglia[6]. Therefore, more studies are focusing on exploring the mechanism of M1 and A1 activation to find targets for therapy[7-9].

Lipocalin 2 (Lcn2), also known as neutrophil gelatinase-associated lipocalin (NGAL), is an acute phase response protein that is upregulated in CNS diseases or injury and plays a regulatory role as an amplifier in neuroinflammation[10-12]. Both in vivo and in vitro studies have shown that Lcn2 is an autocrine mediator of reactive glial cells, which can further promote the activation of microglia and astrocytes and increase the sensitivity of neurons to death signals[13-15]. The Janus kinase-2 (JAK2)-signal transducer and activator of transcription-3 (STAT3) pathway is activated in the CNS injury model according to different degrees of severity of the injury, which regulates the expression of various essential basic functions of genes, including cell proliferation and differentiation, synaptic plasticity, learning and memory, and immunomodulation[16-18]. There is evidence that inhibiting the activation of the JAK2-STAT3 pathway after SCI can effectively reduce secondary injury and promote repair[19-21]. Therefore, targeting the Lcn2 and JAK2-STAT3 pathways, which play a key role in neuroinflammation after SCI, has been verified as one of the treatment strategies[15, 22].

Photobiomodulation (PBM), also known as low-level laser therapy (LLLT), refers to the use of low-energy lasers to irradiate tissues at specific wavelengths of cytochrome c oxidase, enhance mitochondrial function, and improve blood flow and tissue energy metabolism[23, 24]. As an effective method for CNS injury and disease models, PBM has been used in the treatment of traumatic brain injury, stroke, SCI, etc. [25-27]. Previous studies by our team have shown that the application of PBM in an SCI mouse model can affect the polarization of macrophages/microglia, regulate the reactivity of astrocytes, inhibit the formation of glial scars, reduce injured area inflammation, and promote the recovery of motor function[28, 29]. However, the effect of PBM on neurotoxic microglia and astrocytes has not been elucidated. Thus, another purpose of this experiment was to explore the mechanism by which PBM activates M1 and A1 after SCI.

Materials And Methods

Animals

Sprague-Dawley male rats (250–300 g) were supplied by the Animal Center of Air Force Medical University, Xi'an Shaanxi Province, People's Republic of China. The animal experimental protocol was approved by the Animal Protection and Utilization Committee of Air Force Military Medical University. The rats were housed under standard conditions (temperature: 22–25 °C, relative humidity: 45–65%, and 12-h light to dark cycle, with food and water ad libitum). SD rats were randomly divided into three groups: the sham control group, vehicle group and PBM group.

SCI model

Spinal cord injury procedures were established in compliance with the modified bilateral spinal cord clamp model we described before[28]. Briefly, rats were anaesthetized with an intraperitoneal injection of pentobarbital sodium (50 mg/kg). Midline skin incisions were made, the T10 spinous processes were exposed, and a laminectomy was performed at T10. Compression was conducted by placing forceps (Fine Science Tools, Heidelberg, Germany) lateral to the exposed spinal cord. Complete closure was performed with modification by adding a metal spacer between the blades to obtain a gap of 0.5 mm for 40 s. The forceps were removed, and the bleeding was stopped. Then, the muscles and skin were sutured. Throughout the experiment, the rats were placed on a blanket and maintained at a constant temperature of approximately 37 °C. A dose of antibiotic was given by intraperitoneal injection for 5 days after the operation. Urinary retention was relieved by twice-daily bladder expression until the recovery of spontaneous micturition. The sham-operated rats underwent every surgical step except for spinal cord compression, and the laser fibre was implanted beside the lamina in the vehicle group and PBM group.

Laser irradiation

The parameters of the laser irradiation were set according to previous research[28, 30]. Rats were slightly anaesthetized and put into a warm cage, and a continuous 810 nm diode laser (MW-GX-808, Lei Shi Optoelectronics Co., Ltd. Changchun, China, 810 nm wavelength, 150 mW output power) was used in the embedded laser fibre focused on the SCI site. The first irradiation was carried out immediately after injury, and laser treatment was continued for 60 minutes per rat daily for a total of two consecutive weeks in the PBM group. Rats in the sham and vehicle groups were treated identically except for the laser application.

Functional assessment

The Basso-Beattie-Bresnahan (BBB) scale and the Louisville Swimming Scale (LSS) were used to evaluate locomotor function as previously described[31, 32]. The BBB score was evaluated before the operation and 1, 3, 5, 7, 10, 14, 21 and 28 days after injury, and the average score was used in the assessment. Rats are trained to swim from one edge of the glass tank to the other for the swimming test. The LSS was used to assess the movement and alternation of the hind limbs, and the dependence on the

forelimb, body angle and trunk instability were evaluated. Each animal was tested twice. Two observers who were blind to the animal grouping evaluated each animal independently.

RNA-seq analysis

The RNA of the total sample was separated and purified by TRIzol (Invitrogen, Carlsbad, CA, USA) according to the operating protocol provided by the manufacturer. Then, a NanoDrop ND-1000 (NanoDrop, Wilmington, DE, USA) was used to determine the amount and purity of total RNA. The integrity of the RNA was tested by an Agilent 2100, with RIN number >7.0 as the qualified standard, and agarose gel electrophoresis was used for verification. Five micrograms of total RNA was removed, and a Ribo-Zero™ rRNA Removal Kit (Illumina, San Diego, USA) was used to capture and remove ribosomal RNA according to the standard operating procedures. Then, the linear RNA was removed by the action of RNase R (Epicentre Inc, Madison, WI, USA), and the remaining RNA was fragmented with divalent cations at high temperature. Reverse transcriptase was used to synthesize cDNA from the fragmented RNA. Then, *E. coli* DNA polymerase I and RNase H were used for two-strand synthesis to convert these double-stranded DNA and RNA complexes into double-stranded DNA. At the same time, DUTP was incorporated into the two strands to blunt the ends of the double-stranded DNA. Then, an A base was added at each end so that the DNA could be connected to a linker with a T base at the end, and magnetic beads were used to screen and purify by fragment size. The two strands were digested with UDG, and then PCR was used to form a library with a fragment size of 300 bp (±50 bp). Finally, we used an Illumina HiSeq 4000 (LC Bio, China) to perform paired-end sequencing according to the standard operation.

Tissue processing

Rats were perfused with paraformaldehyde in phosphate buffer (4%, 4 °C, pH 7.4), and a 2 cm long spinal cord segment was carefully dissected from the centre of the injury site and placed in the same fixation solution within 4~6 h. Then, the transferred cord was placed in 25% glucose phosphate buffer at 4 °C until it sank. Afterward, 10 μm serial sagittal sections were cut with a cryostat (CM1900, Leica, Germany) and carefully mounted on slides for 10 cyclic sets.

Immunofluorescence

Sections were rinsed three times in phosphate-buffered saline (PBS) for 5 minutes each. Then, the sections were blocked with 1% donkey serum containing 0.3% Triton X-100 at room temperature for 30 minutes. The sections were then incubated at 4 °C with the primary antibodies overnight and with appropriate secondary antibodies at 37 °C for 2 h. Finally, to label the nuclei, the sections were counterstained with 4',6-diamidino-2-phenylindole (DAPI). Images were taken under a fluorescence microscope (BX51, Olympus, Tokyo, Japan). The following primary antibodies were used: anti-C3 (1:300, Abcam, ab200999), anti-Lcn2 (1:200, Abcam, ab63929), anti-GFAP (1:400, ab4674, Abcam), anti-Iba1 (1:500, Abcam, ab178846), anti-iNOS (1:500, Abcam, ab49999), and anti-NeuN (1:100, Abcam, ab177487).

TUNEL staining

The TUNEL kit was purchased from Beyotime (Nanjing, China), and the experimental process was performed in accordance with the manufacturer's protocol. The proportion of TUNEL-positive cells was assessed. Fluorescence images were captured with a BX51 fluorescence microscope (Olympus, Tokyo, Japan).

Primary cell cultures

The cerebral cortex of 1~3-day-old rats was carefully dissected into slices 0.5~1 mm thick. The slices were placed in 0.125% trypsin EDTA solution (Thermo Fisher Science) and shaken gently for 20 minutes. The digested tissue was centrifuged at 300 × g for 5 minutes and resuspended in DMEM/F12 (Gibco). After filtration with 100m nylon mesh, the final single-cell suspension was cultured in a T75 culture flask that was precoated with poly-L-lysine (Sigma Aldrich). The medium was changed the next day and then every three days. After culturing in vitro for 12~14 days, the culture flasks were shaken at 200 rpm for 2 h, and then mature microglia were obtained from the supernatant. The remaining astrocytes were digested with trypsin and re-cultured for follow-up experiments.

Cell treatment

Primary microglia were induced to adopt the M1 phenotype in culture medium with 10% foetal bovine serum (FBS), 1% DMEM, 1μg/ml lipopolysaccharide (Sigma Aldrich) and 20 ng/ml IFN-gamma (IFN-γ) (Sigma Aldrich) for 24 h. A1 astrocytes were induced with C1q (400 ng/ml, MyBioSource, MBS 143105), TNF - α (30 ng/ml, Cell Signaling Technology, 8902SF) and IL-1 α (3 ng/ml, Sigma, i3901) for 24 h. After induction, the supernatants were collected as microglia conditioned medium (MCM) and astrocyte conditioned medium (ACM). The culture system was immediately treated with PBM (810 nm, 6 mW, 4.5 cm^2, 8 minutes) after induction and then irradiated twice every 12 h. Cucurbitacin I (0.5 μM, MedChem Express, NJ, USA) and recombinant Lcn2 protein (1 μg/ml, R&D Systems) were added to the culture medium of microglia and astrocytes with induced polarization. Adenovirus carrying the LCN2 gene at a multiplicity of infection (MOI) of 20 was purchased from HanBio (Shanghai, China). Transfection was performed according to the manufacturer's instructions for 24 h. Virus lacking a target sequence (empty vector) was used as a control, and the level of knockdown was detected by RT-PCR and Western blot.

Flow cytometry

Ventral spinal cord 4.1 (VSC4.1) was cocultured with MCM and ACM for 24 h, apoptosis was detected by flow cytometry with an Annexin V-FITC apoptosis detection kit (Thermo Fisher) according to the manufacturer's protocol, and 1% bovine serum albumin (BSA) was used to block nonspecific antibody binding. Cells were analysed with a Beckman F500 flow cytometer, and in each sample, at least 10,000 cells were analysed. FlowJo software (TreeStar, San Carlos, CA, USA) was used to analyse the results.

ELISA

The rats were sacrificed under deep anaesthesia, and 2 cm injured spinal segments were immediately removed and homogenized in PBS. The supernatants of tissue homogenates were collected and analysed using rat IL-1α, TNF-α, and C1q (Jiangsu Meimian Industrial Co., Ltd.) ELISA kits according to the manufacturer's instructions.

RT-PCR

Total RNA was extracted with a commercial RNA extraction kit (Takara Bio, Inc., Shiga, Japan) according to the manufacturer's protocol. The RNA integrity was evaluated, and purified RNAs with RIN scores > 7 were reverse transcribed. The cDNA was reverse transcribed from 1 μg of RNA template with the PrimeScript RT Master Mix Kit (Takara bio, Inc.). Real-time fluorescent PCR was performed in 10 μL of solution containing 1.5 μL of cDNA, 2.5 μL of ddH2O, 1 μL of primer and 5 μL of SYBR Green according to the manufacturer's instructions. Clean reads were obtained after removing low-quality reads and those containing adapter and poly-N sequences. The GAPDH gene was used as internal reference. The RT-qPCR data were analysed by the $2^{-\Delta\Delta CT}$ method. The sequences of the primer pairs for target genes are as shown below:

Table 1 RT-PCR primer sequences

Gene	Forward primer sequence (5'–3')	Reverse primer sequence (5'–3')
Lcn2	CCGACACTGACTACGACCAG	AATGCATTGGTCGGTGGGAA
iNOS	TGGTGAGGGGACTGGACTTT	ATCCTGTGTTGTTGGGCTGG
C3	CCAGCTCCCCATTAGCTCTG	GCACTTGCCTCTTTAGGAAGTC
Gfap	AACCGCATCACCATTCCTGT	TCCTTAATGACCTCGCCATCC
Amigo2	GTTCGCCACAACAACATCAC	GTTTCTGCAAGTGGGAGAGC
Serping1	TGGCTCAGAGGCTAACTGGC	GAATCTGAGAAGGCTCTATCCCCA
C1q	TCTGCACTGTACCCGGCTA	CCCTGGTAAATGTGACCCTTTT
IL-1α	GCACCTTACACCTACCAGAGT	AAACTTCTGCCTGACGAGCTT
TNF-α	CCCTCACACTCAGATCATCTTCT	GCTACGACGTGGGCTACAG
IL-6	ATTGTATGAACAGCGATGATGCAC	CCAGGTAGAAACGGAACTCCAG
IL-1β	CCCTGAACTCAACTGTGAAATAGCA	CCCAAGTCAAGGGCTTGGAA
GADPH	GAACATCATCCCTGCATCCA	CCAGTGAGCTTCCCGTTCA

Western blot

Total protein was extracted using radioimmunoprecipitation assay (RIPA) lysis and extraction buffer, which included a protease inhibitor cocktail. The concentration of protein was determined by the BCA method. Equal amounts of protein from each sample were separated using 8% or 10% SDS-PAGE and transferred to NC membranes (EMD Millipore Corp, Burlington, MA). The membranes were blocked with 5% bovine serum albumin for 1 h at room temperature and then incubated overnight at 4 °C with the following specific primary antibodies: rabbit anti-iNOS (18985-1-AP, Proteintech, 1:1000), rabbit anti-C3 (ab200999, Abcam, 1:1000), rabbit anti-GFAP (SAB4300647, Sigma, 1:1000), rabbit anti-JAK2 (3230, Cell Signaling Technology, 1:1000), rabbit anti-pJAK2 (AF3022, Affinity, 1:1000), rabbit anti-STAT3 (12640, Cell Signaling Technology, 1:1000), rabbit anti-pSTAT3 (ab76315, Abcam, 1:1000), rabbit anti-Lcn2 (ab63929, Abcam, 1:1000), β-actin (66009-1-Ig, Proteintech, 1:1000). After incubation with the corresponding secondary antibodies (1:2000) for 1 h at room temperature, the membranes were scanned with ECL-Plus Reagent (Millipore, Billerica, MA, United States) and observed under an Amersham Imager 600 (General Electric, United States).

Statistical analysis

At least three independent biological replicates were performed. All data were presented as means ± standard deviation. Statistical analysis was performed with GraphPad Prism 8 software. Student's t-test was used for comparisons between two groups. For multiple comparisons, the data were analysed by one-way ANOVA followed by Bonferroni's post hoc test. BBB scales and LSS scores were assessed by two-way ANOVA. Statistical significance was defined at $p \leq 0.05$.

Results

1. **The effect of PBM on the dynamic changes in microglia and astrocytes after SCI.**

We first observed the distribution and activation of microglia and astrocytes in spinal cord tissue at different days post injury (dpi) in the vehicle and PBM groups. (Fig 1.a). The normal and complete tissue structure was destroyed, and microglia began to activate and proliferate within 24 h after SCI. At 3 dpi, a large number of ionized calcium binding adapter molecule 1 (Iba1)-positive cells (microglia) were recruited to the damaged area, and the number of microglia peaked at 7 dpi. Subsequently, inflammation began to enter the subacute phase, the number of microglia began to decline, astrocytes begin to significantly upregulate the expression of glial fibrillary acidic protein (GFAP), and the two types of glial cells jointly participated in scar formation. At 28 dpi, the spinal cord cavity began to form, and the scar structure became denser. Compared with vehicle treatment, PBM treatment downregulated the number of microglia and the expression of GFAP post injury (Fig 1.b, c).

We investigated the mRNA expression of C3 and iNOS after SCI by RT-PCR, and the results suggested that the peak expression of C3 began to appear at 7 dpi, and PBM suppressed this upregulation trend (Fig 1.d). The level of iNOS immediately increased at 1 dpi and then gradually decreased. PBM significantly inhibited the upregulation of iNOS at 3 dpi (Fig 1.e).

2. **PBM inhibits the activation of neurotoxic microglia after SCI.**

Considering that the activation of microglia is more obvious in the acute phase after injury, we first observed changes in microglia after early PBM intervention (Fig 2.a). At 3 dpi, a large number of microglia had high iNOS (M1 type) expression in the injury epicentre in the vehicle group, while the intensity of iNOS in the PBM group became weaker ($p<0.05$). Western blot assays showed the same results ($p<0.01$; Fig 2. b). At 7 dpi and 14 dpi, we also observed that the intensity of iNOS in the PBM group was lower than that in the vehicle group, but there was no significant difference between the two groups.

There were differences in the spatial distribution of microglia after SCI. We separately counted the number of microglia at distances of 150 μm, 300 μm, and 600 μm from the epicentre to the rostral or caudal sides at 3 dpi. The results showed that PBM reduced the number of microglia at 150 μm in the rostral and caudal directions of the spinal cord from the epicentre ($p<0.05$, $p<0.05$; Fig 2.c).

We next investigated the morphology of microglia 150 μm from the centre of the injury area. Ramified microglia are resting microglia, while bushy and hypertrophic microglia represent typical activated microglia. In the sham group, ramifications with smaller cell diameters and more bifurcations were dominant. After injury, most of the microglial cell branches were reduced, the cell body was hypertrophic, the proportion of bushy and hypertrophic microglial cells was increased, and PBM intervention reduced the ratio of the two types of cells after injury (Fig. 2d,e).

3. **PBM inhibits the activation of A1 astrocytes after SCI.**

A1 astrocytes are induced by C1q, IL-1α and TNF-α secreted by activated microglia. We investigated the protein expression levels in the injured spinal cord tissue at 3 dpi, and the ELISA results showed that the levels of C1q, IL-1α and TNF-α after injury were significantly higher than those in the sham group ($p<0.001$, $p<0.01$, $p<0.001$), and PBM treatment inhibited the increasing trend ($p<0.01$, $p<0.01$, $p<0.01$; Fig. 3e-h).

At 7 dpi, A1 astrocytes were clearly activated, and a large number of C3-positive cells appeared in the injured area (Fig 3.a). As the injury course entered the subacute phase, the expression of C3 was also upregulated and basically colocalized only with GFAP-positive cells. After PBM intervention, the expression levels of C3 and GFAP (7 dpi, $p<0.05$; 14 dpi, $p<0.05$; 28 dpi, $p<0.05$; Fig 3.b) were effectively inhibited. Western blot assays also showed that the C3 and GFAP protein levels in the PBM group were lower than those in the sham group at 7 dpi ($p<0.01$, $p<0.01$; Fig 2.i). However, we measured the length of processes and the diameter of the cell body of astrocytes, and there was no significant difference between the vehicle group and the PBM group at 3 dpi, 7 dpi, and 14 dpi.

4. **PBM can reduce apoptosis, increase the number of surviving neurons and promote the recovery of motor function after SCI.**

Next, we investigated tissue apoptosis in the injured area and found that apoptosis mainly occurred in the acute phase postinjury. As shown in Fig 4.a, there were basically no TUNEL-positive cells in uninjured

spinal cord tissue. At 1 dpi, 3 dpi and 7 dpi, the proportions of TUNEL-positive cells were 47.84%±6.09%, 39.91%±3.35% and 5.48%±1.35%, respectively. After PBM treatment, this proportion became 30.40% ±6.39% ($p<0.05$), 23.91%±4.90% ($p<0.05$) and 2.58%±0.69% ($p<0.05$). We counted the number of spinal ventral motor neurons in the parainjury site, and the results showed that the number of retained neurons in the PBM group was greater than that in the vehicle group at 7 dpi (PBM group vs vehicle group, 90.00±5.57 vs 72.67±5.03, $p<0.05$; Fig 4.b). Similarly, at 14 dpi and 28 dpi, the ability to retain the number of motor neurons in the para region after injury was significantly different between the PBM group and the vehicle group ($p<0.05$; $p<0.05$).

To evaluate the effect of PBM treatment on the recovery of motor function after SCI, we comprehensively considered two scales, the BBB score and LSS score. The BBB score results showed that the difference between the PBM group and the vehicle group began to appear at 7 dpi and continued until 28 dpi (Fig 5.c). The LSS scale showed the same results, and the score in the PBM group was higher than that in the vehicle group (7 dpi, $p<0.05$; 14 dpi, $p<0.01$; 28 dpi, $p<0.01$) (Fig 5.d).

5. **PBM inhibits the expression of Lcn2 and the activation of the JAK2-STAT3 pathway after SCI.**

Within 24 h after SCI, a large amount of pro-inflammatory factors were released from the injured area, causing a cascade of inflammatory storms. Microarray analysis showed that 1,379 genes were upregulated and 168 genes were downregulated in the SCI and sham groups at 1 dpi, and Lcn2 was one of the significantly upregulated genes (Fig 4.a, b).

We next checked the expression of Lcn2 in the tissues on different days after injury. The RT-PCR results showed that the expression level of Lcn2 in the SCI group was significantly increased at 1 dpi ($P<0.01$; Fig 4.c). The results of immunofluorescence staining also showed that Lcn2 was significantly upregulated at 1 dpi, and it was secreted to the entire injury area and the para-injury area (Fig 4.d). Subsequently, the level of Lcn2 decreased and was distributed only near the injured area at 7 dpi. At 14 dpi and 28 dpi, Lcn2 was rarely secreted and basically was present only in astrocytes and colocalized only with GFAP. On different days after injury, the fluorescence intensity of Lcn2 in the PBM group was lower than that in the vehicle group.

Considering the important role of JAK2-STAT3 signalling pathway activation in the regulation of Lcn2 and in glial cell activation after SCI, we examined the activation of the JAK2-STAT3 pathway in the PBM group and the vehicle group. Western blot results showed that the activation time course of the JAK2-STAT3 pathway after SCI paralleled Lcn2 expression, and PBM inhibited the activation of the JAK2-STAT3 signal pathway, which was consistent with the suppression of Lcn2 (Fig 4.f).

6. **PBM inhibits the activation of M1 microglia and A1 astrocytes in vitro.**

We isolated primary cultured microglia and astrocytes in vitro. Lipopolysaccharide (LPS) and IFN-γ were used to induce the polarization of microglia to the M1 type, and C1q, TNF-α and IL-1α were used to induce the polarization of astrocytes to A1s. Then, laser irradiation was used to irradiate the culture system to

verify the effect of PBM on neurotoxic glial cells. The immunofluorescence results showed that the expression of iNOS in M1 microglia was significantly upregulated, and PBM intervention inhibited the increase in the expression of iNOS (Fig 6.a). The Western blot results also showed that PBM inhibited the upregulation of iNOS in M1 microglia ($p<0.0001$, $p<0.001$; Fig 6. b). RT-PCR results showed that inflammatory factors such as iNOS, IL-6, and IL-β ($p<0.0001$), as well as C1q, IL-1α, and TNF-α ($p<0.01$), were significantly upregulated after induction, and PBM intervention inhibited the upregulation of inflammatory indicators ($p<0.01$, $p<0.05$; Fig 6.c, d).

Immunofluorescence staining and Western blot analysis showed that in addition to the high expression of C3 in A1 astrocytes in vitro ($p<0.0001$), the expression of Lcn2 increased significantly ($p<0.0001$). After PBM treatment, the increase in C3 and Lcn2 was inhibited ($p<0.01$; $p<0.001$; Fig 6. e, f). We also checked the A1-specific transcripts Amigo2 and Serping1, and similar to the expression of C3 and Lcn2, PBM treatment blocked the high mRNA expression of these molecules in A1s (Fig 6.g).

We used the VSC4.1 cell line to verify whether PBM can attenuate the neurotoxic effects of M1 microglia and A1 astrocytes. We added M1 MCM and A1 astrocyte culture medium (ACM) to the VSC4.1 culture system for 24 h. The results showed that MCM was added to VSC4.1 before and after PBM intervention and had basically no effect on neuronal apoptosis compared with the control group (data not shown), while when ACM was added to VSC4.1, the flow cytometry showed that the neuronal apoptosis rate in the ACM group was 10.43%±0.45% (vs control group 0.76%±0.15%, $p<0.0001$). After PBM intervention, ACM was added to the VSC4.1 culture system, and the apoptosis rate became 5.17%±0.57% ($p<0.001$; Fig 6.h).

7. **PBM can interfere with Lcn2/JAK2-STAT3 crosstalk during the activation of neurotoxic glial cells in vitro.**

The results of animal experiments suggest that the mechanism of PBM may be related to the inhibition of the high expression of Lcn2 and the activation of the JAK2-STAT3 signalling pathway after SCI. To explore the relationship between the two and the suppression of M1 and A1, we designed in vitro experiments. First, we used cucurbitacin I (a specific inhibitor of JAK2-STAT3) in vitro to block the activation of the JAK2-STAT3 pathway during M1 and A1 activation. Similar to the effect of PBM, the application of cucurbitacin I alone can reduce the levels of C3 and iNOS while also reducing the increase in Lcn2. The combined application of the two can further enhance the effect of inhibiting M1 and A1 (Fig 7.a, b).

Next, we used adenovirus transfection and recombinant protein to apply to the culture system of microglia and astrocytes to change the level of Lcn2. The results showed that in microglia and astrocytes that were not induced, the level of Lcn2 and the activation of JAK2-STAT3 were relatively low, and adenovirus transfection effectively reduced the level of Lcn2. However, after the application of PBM and ReLcn2 to resting microglia and astrocytes, respectively, there were no significant changes in the expression of Lcn2, activation of JAK2-STAT3, or level of C3 (or iNOS). In M1 microglia and A1 astrocytes, knocking down Lcn2 alone can inhibit the high expression of C3 (or iNOS), and at the same time, the activation of the JAK2-STAT3 pathway is blocked. The addition of ReLcn2 to the culture system

further increased the degree of activation of JAK2-STAT3 and markers of neurotoxic glial cells. After the joint application of PBM intervention, PBM enhanced the inhibitory effect of sh-Lcn2, while ReLcn2 can weaken the effect of PBM (Fig 7.c, d).

Discussion

In this study, we found that the activation of microglia and astrocytes has a time course after SCI. In the acute phase (within 7 dpi), resting microglia are activated immediately postinjury, begin to proliferate and migrate to the epicentre of the injury, and their morphology changes from a ramified state to a bushy state or to a hypertrophic state, secreting proinflammatory factors, including C1q, IL-1α and TNF-α, to further amplify the cascade of neuroinflammation. As the disease progresses into the subacute phase, the degree of microglial activation begins to decrease, and then astrocytes begin to activate. As a marker of A1 astrocytes, the expression of C3 began to be significantly upregulated at 7 dpi and strengthened in the following 28 dpi. Therefore, we conclude that neurotoxic microglia and astrocytes are activated in succession in the acute and subacute phases of SCI, and both of them are involved in secondary neuroinflammation, which is consistent with previous reports[33, 34]. In view of the fact that little is known about the activation of M1 and A1, we tried to identify the underlying mechanism through RNA-seq analysis. The results showed that the expression of Lcn2 was significantly upregulated at 1 dpi, and this phenomenon was also verified by RT-PCR, which is consistent with previous research reports[15, 35]. Interestingly, the time course of activation of the JAK2-STAT3 signalling pathway after SCI was consistent with the change in the level of Lcn2. Previous research has confirmed that Lcn2 secreted under inflammatory conditions can recruit more inflammatory cells through activation of the JAK2-STAT3 signalling pathway, causing upregulation and secretion of chemokines and thereby amplifying neuroinflammation[10]. Other studies have shown that reactive astrogliosis depends on the activation of STAT3. Lcn2 is a STAT3-dependent upregulator of astrocytes and is involved in the regulation of chronic pruritus[36]; cytokines activated by STAT3 can enhance the expression of Lcn2[37, 38]. Lcn2 secreted by activated microglia and astrocytes can further enhance the activation of M1 and A1[39, 40], and the activation of the JAK2-STAT3 pathway is also necessary in neuroinflammation involving the participation of microglia and astrocytes. Inhibiting the JAK2-STAT3 pathway can also reduce the reactivity of glial cells[41-43]. Therefore, combined with the in vivo experimental results, we hypothesize that there may be a connection between the Lcn2 and JAK2-STAT3 pathways in the activation of M1 and A1 after SCI.

Subsequently, in vitro experiments were conducted to explore the role of the Lcn2 and JAK2-STAT3 pathways in the activation of M1 and A1. We first used a JAK2-STAT3 signalling pathway inhibitor (cucurbitacin I) to be added to the culture system of M1 and A1. The results showed that cucurbitacin I can effectively inhibit the upregulation of JAK2-STAT3 in the activation of M1 and A1, and at the same time, the increased expression of C3 and iNOS was also suppressed. Next, we used adenovirus containing shRNA to transfect microglia and astrocytes separately to knock down Lcn2 and found that the activation of M1 and A1 was suppressed and the activation of the JAK2-STAT3 pathway was also blocked. Moreover, adding recombinant Lcn2 protein to the culture system of M1 and A1 further enhanced the level of the JAK2-STAT3 pathway and the degree of activation of M1 and A1. However,

ReLcn2 at certain concentrations had no significant effect on the Lcn2 and JAK2-STAT3 pathways in resting microglia and astrocytes and could not effectively promote the activation of M1 and A1. However, there are reports that higher levels of ReLcn2 can cause the activation of microglia and astrocytes[12, 44, 45]. Therefore, we believe that only in the condition of inducing resting microglia and astrocytes to M1 and A1 can the level of Lcn2 affect the activation of the JAK2-STAT3 pathway and further affect the activation of M1 and A1. The Lcn2 and JAK2-STAT3 pathways jointly participate in the activation process of M1 and A1, and the two have a crosstalk of mutual regulation, which can promote each other to enhance the activation degree of M1 and A1. The crosstalk of Lcn2/JAK2-STAT3 in the activation of M1 and A1 provides a better understanding of neuroinflammation.

Due to the complexity of the pathophysiological process of SCI and the timing of the intervention window, many current treatments have unclear mechanisms and large side effects that limit their clinical applications[46, 47]. In this study, we tried to verify an optimized PBM treatment by embedding biocompatible laser fibres next to the vertebral body in the process of modelling SCI based on previous studies[30, 48] to better project laser energy to the surface of the injured spinal cord. Continuous irradiation every day after SCI and PBM can effectively play a therapeutic role in both the acute and subacute phases, leading to better motor function recovery outcomes. To our knowledge, this study is the first to investigate the mechanism of PBM by implanting a laser fibre in an SCI model in vivo. In short, we proposed a new mechanism of M1 and A1 activation in an SCI model and verified the therapeutic effect of PBM on M1 and A1 both in vivo and in vitro. We look forward to this work providing new insight into a better understanding of targeting M1 and A1 as intervention strategies in the future.

Conclusion

In this study, we discovered the activation time course of neurotoxic microglia and astrocytes after SCI and proved that the crosstalk of Lcn2/JAK2-STAT3 is involved in this process. At the same time, it was verified that PBM can inhibit the activation of M1 and A1 by inhibiting the Lcn2/JAK2-STAT3 interaction, thereby promoting the recovery of SCI.

Abbreviations

PBM, Photobiomodulation; SCI, spinal cord injury; CNS, central nervous system; GFAP, glial fibrillary acidic protein; Iba1, ionized calcium binding adapter molecule 1; JAK2-STAT3, Janus kinase 2-Signal transducer and activator of transcription 3; M1, M1 type microglia; A1(s), A1 type astrocyte; Lcn2, lipocalin 2; iNOS, inducible nitric oxide synthase; TNF- α, tumor necrosis factor-α; IL-1β, interleukin-1β; IL-6, interleukin-6; IL-1α, interleukin-1α; C1q, complement component 1q.

Declarations

Ethics approval and consent to participate

All procedures involving animals were approved by the Institutional Animal Care and Use Committee at Air Force Military Medical University.

Consent for publication

All authors consent this article for publication.

Availability of data and materials

All raw data used in this manuscript are available on reasonable request.

Competing interests

The authors declare that they have no competing interests.

Funding

This work was supported by National Natural Scientific Foundation of China Grant (NO.81070996, NO.81572151), Shaanxi Provincial Key R&D Program, China (NO.2020ZDLSF02-05, NO.2021ZDLSF02-10, NO. 2021SF-029), Everest Project of Military Medicine of Air Force Military Medical University(2018RCFC02).

Authors' Contributions

XW, XL, XH, and ZW designed and conceived the study. XL, ZL, TD and XW built the animal model and conducted PBM intervention. XW, XL, XZ, ZL, KL, YM, PL, ZZ, JW, ZS, HQ and ZZ performed the experiments. XK, CJ, and ZZ contributed to analysis. The manuscript was written by XW, XH, and ZW, XH and ZW critically contributed to and revised the manuscript.

References

1. Global, regional, and national burden of neurological disorders, 1990-2016: a systematic analysis for the Global Burden of Disease Study 2016. Lancet Neurol. 2019; 18: 459-80.
2. Wyss-Coray T, Mucke L. Inflammation in neurodegenerative disease--a double-edged sword. Neuron. 2002; 35: 419-32.
3. Vainchtein ID, Molofsky AV. Astrocytes and Microglia: In Sickness and in Health. Trends in neurosciences. 2020; 43: 144-54.
4. Kwon HS, Koh SH. Neuroinflammation in neurodegenerative disorders: the roles of microglia and astrocytes. Translational neurodegeneration. 2020; 9: 42.
5. Pisanu A, Lecca D, Mulas G, Wardas J, Simbula G, Spiga S, et al. Dynamic changes in pro- and anti-inflammatory cytokines in microglia after PPAR-γ agonist neuroprotective treatment in the MPTPp mouse model of progressive Parkinson's disease. Neurobiology of disease. 2014; 71: 280-91.

6. Liddelow SA, Guttenplan KA, Clarke LE, Bennett FC, Bohlen CJ, Schirmer L, et al. Neurotoxic reactive astrocytes are induced by activated microglia. Nature. 2017; 541: 481-7.
7. Zheng J, Lu J, Mei S, Wu H, Sun Z, Fang Y, et al. Ceria nanoparticles ameliorate white matter injury after intracerebral hemorrhage: microglia-astrocyte involvement in remyelination. J Neuroinflammation. 2021; 18: 43.
8. Jiang D, Gong F, Ge X, Lv C, Huang C, Feng S, et al. Neuron-derived exosomes-transmitted miR-124-3p protect traumatically injured spinal cord by suppressing the activation of neurotoxic microglia and astrocytes. Journal of nanobiotechnology. 2020; 18: 105.
9. He J, Liu H, Zhong J, Guo Z, Wu J, Zhang H, et al. Bexarotene protects against neurotoxicity partially through a PPARγ-dependent mechanism in mice following traumatic brain injury. Neurobiology of disease. 2018; 117: 114-24.
10. Lee S, Kim JH, Kim JH, Seo JW, Han HS, Lee WH, et al. Lipocalin-2 Is a chemokine inducer in the central nervous system: role of chemokine ligand 10 (CXCL10) in lipocalin-2-induced cell migration. The Journal of biological chemistry. 2011; 286: 43855-70.
11. Jha MK, Jeon S, Jin M, Ock J, Kim JH, Lee WH, et al. The pivotal role played by lipocalin-2 in chronic inflammatory pain. Experimental neurology. 2014; 254: 41-53.
12. Lee S, Lee J, Kim S, Park JY, Lee WH, Mori K, et al. A dual role of lipocalin 2 in the apoptosis and deramification of activated microglia. Journal of immunology (Baltimore, Md : 1950). 2007; 179: 3231-41.
13. Lee S, Park JY, Lee WH, Kim H, Park HC, Mori K, et al. Lipocalin-2 is an autocrine mediator of reactive astrocytosis. The Journal of neuroscience : the official journal of the Society for Neuroscience. 2009; 29: 234-49.
14. Bi F, Huang C, Tong J, Qiu G, Huang B, Wu Q, et al. Reactive astrocytes secrete lcn2 to promote neuron death. Proceedings of the National Academy of Sciences of the United States of America. 2013; 110: 4069-74.
15. Braga A, Bandiera S, Verheyen J, Hamel R, Rutigliani C, Edenhofer F, et al. Combination of In Situ Lcn2 pRNA-RNAi Nanotherapeutics and iNSC Transplantation Ameliorates Experimental SCI in Mice. Molecular therapy : the journal of the American Society of Gene Therapy. 2020; 28: 2677-90.
16. Shyu WC, Lin SZ, Chiang MF, Chen DC, Su CY, Wang HJ, et al. Secretoneurin promotes neuroprotection and neuronal plasticity via the Jak2/Stat3 pathway in murine models of stroke. The Journal of clinical investigation. 2008; 118: 133-48.
17. Nicolas CS, Peineau S, Amici M, Csaba Z, Fafouri A, Javalet C, et al. The Jak/STAT pathway is involved in synaptic plasticity. Neuron. 2012; 73: 374-90.
18. Shan Y, Tan S, Lin Y, Liao S, Zhang B, Chen X, et al. The glucagon-like peptide-1 receptor agonist reduces inflammation and blood-brain barrier breakdown in an astrocyte-dependent manner in experimental stroke. J Neuroinflammation. 2019; 16: 242.
19. Zheng XQ, Huang JF, Lin JL, Zhu YX, Wang MQ, Guo ML, et al. Controlled release of baricitinib from a thermos-responsive hydrogel system inhibits inflammation by suppressing JAK2/STAT3 pathway in

acute spinal cord injury. Colloids and surfaces B, Biointerfaces. 2020; 199: 111532.

20. Fu XM, Wang Y, Fu WL, Liu DH, Zhang CY, Wang QL, et al. The Combination of Adipose-derived Schwann-like Cells and Acellular Nerve Allografts Promotes Sciatic Nerve Regeneration and Repair through the JAK2/STAT3 Signaling Pathway in Rats. Neuroscience. 2019; 422: 134-45.
21. Li JW, Kuang Y, Chen L, Wang JF. LncRNA ZNF667-AS1 inhibits inflammatory response and promotes recovery of spinal cord injury via suppressing JAK-STAT pathway. Eur Rev Med Pharmacol Sci. 2018; 22: 7614-20.
22. Zheng XQ, Huang JF, Lin JL, Zhu YX, Wang MQ, Guo ML, et al. Controlled release of baricitinib from a thermos-responsive hydrogel system inhibits inflammation by suppressing JAK2/STAT3 pathway in acute spinal cord injury. Colloids and surfaces B, Biointerfaces. 2021; 199: 111532.
23. Chen AC, Arany PR, Huang YY, Tomkinson EM, Sharma SK, Kharkwal GB, et al. Low-level laser therapy activates NF-kB via generation of reactive oxygen species in mouse embryonic fibroblasts. PLoS One. 2011; 6: e22453.
24. Bayat M, Abdi S, Javadieh F, Mohsenifar Z, Rashid MR. The effects of low-level laser therapy on bone in diabetic and nondiabetic rats. Photomedicine and laser surgery. 2009; 27: 703-8.
25. Svobodova B, Kloudova A, Ruzicka J, Kajtmanova L, Navratil L, Sedlacek R, et al. The effect of 808 nm and 905 nm wavelength light on recovery after spinal cord injury. Sci Rep. 2019; 9: 7660.
26. Salehpour F, Farajdokht F, Mahmoudi J, Erfani M, Farhoudi M, Karimi P, et al. Photobiomodulation and Coenzyme Q10 Treatments Attenuate Cognitive Impairment Associated With Model of Transient Global Brain Ischemia in Artificially Aged Mice. Frontiers in cellular neuroscience. 2019; 13: 74.
27. Morries LD, Cassano P, Henderson TA. Treatments for traumatic brain injury with emphasis on transcranial near-infrared laser phototherapy. Neuropsychiatric disease and treatment. 2015; 11: 2159-75.
28. Song JW, Li K, Liang ZW, Dai C, Shen XF, Gong YZ, et al. Low-level laser facilitates alternatively activated macrophage/microglia polarization and promotes functional recovery after crush spinal cord injury in rats. Sci Rep. 2017; 7: 620.
29. Sun J, Zhang J, Li K, Zheng Q, Song J, Liang Z, et al. Photobiomodulation Therapy Inhibit the Activation and Secretory of Astrocytes by Altering Macrophage Polarization. Cell Mol Neurobiol. 2020; 40: 141-52.
30. Liang Z, Lei T, Wang S, Zuo X, Li K, Song J, et al. Photobiomodulation by diffusing optical fiber on spinal cord: A feasibility study in piglet model. Journal of biophotonics. 2019: e201960022.
31. Basso DM, Beattie MS, Bresnahan JC. A sensitive and reliable locomotor rating scale for open field testing in rats. Journal of neurotrauma. 1995; 12: 1-21.
32. Smith RR, Burke DA, Baldini AD, Shum-Siu A, Baltzley R, Bunger M, et al. The Louisville Swim Scale: a novel assessment of hindlimb function following spinal cord injury in adult rats. Journal of neurotrauma. 2006; 23: 1654-70.
33. Zrzavy T, Schwaiger C, Wimmer I, Berger T, Bauer J, Butovsky O, et al. Acute and non-resolving inflammation associate with oxidative injury after human spinal cord injury. Brain. 2021; 144: 144-

61.

34. Qian D, Li L, Rong Y, Liu W, Wang Q, Zhou Z, et al. Blocking Notch signal pathway suppresses the activation of neurotoxic A1 astrocytes after spinal cord injury. Cell Cycle. 2019; 18: 3010-29.
35. Rathore KI, Berard JL, Redensek A, Chierzi S, Lopez-Vales R, Santos M, et al. Lipocalin 2 plays an immunomodulatory role and has detrimental effects after spinal cord injury. The Journal of neuroscience : the official journal of the Society for Neuroscience. 2011; 31: 13412-9.
36. Shiratori-Hayashi M, Koga K, Tozaki-Saitoh H, Kohro Y, Toyonaga H, Yamaguchi C, et al. STAT3-dependent reactive astrogliosis in the spinal dorsal horn underlies chronic itch. Nat Med. 2015; 21: 927-31.
37. Zhang Y, Liu J, Yang B, Zheng Y, Yao M, Sun M, et al. Ginkgo biloba Extract Inhibits Astrocytic Lipocalin-2 Expression and Alleviates Neuroinflammatory Injury via the JAK2/STAT3 Pathway After Ischemic Brain Stroke. Front Pharmacol. 2018; 9: 518.
38. Zhang Y, Liu J, Yao M, Song W, Zheng Y, Xu L, et al. Sailuotong Capsule Prevents the Cerebral Ischaemia-Induced Neuroinflammation and Impairment of Recognition Memory through Inhibition of LCN2 Expression. Oxidative medicine and cellular longevity. 2019; 2019: 8416105.
39. Jang E, Lee S, Kim JH, Kim JH, Seo JW, Lee WH, et al. Secreted protein lipocalin-2 promotes microglial M1 polarization. FASEB journal : official publication of the Federation of American Societies for Experimental Biology. 2013; 27: 1176-90.
40. Lee S, Jha MK, Suk K. Lipocalin-2 in the Inflammatory Activation of Brain Astrocytes. Critical reviews in immunology. 2015; 35: 77-84.
41. Ceyzériat K, Ben Haim L, Denizot A, Pommier D, Matos M, Guillemaud O, et al. Modulation of astrocyte reactivity improves functional deficits in mouse models of Alzheimer's disease. Acta neuropathologica communications. 2018; 6: 104.
42. Mai HN, Nguyen LTT, Shin EJ, Kim DJ, Jeong JH, Chung YH, et al. Astrocytic mobilization of glutathione peroxidase-1 contributes to the protective potential against cocaine kindling behaviors in mice via activation of JAK2/STAT3 signaling. Free radical biology & medicine. 2019; 131: 408-31.
43. Shu M, Zhou Y, Zhu W, Wu S, Zheng X, Yan G. Activation of a pro-survival pathway IL-6/JAK2/STAT3 contributes to glial fibrillary acidic protein induction during the cholera toxin-induced differentiation of C6 malignant glioma cells. Molecular oncology. 2011; 5: 265-72.
44. Jang E, Kim JH, Lee S, Kim JH, Seo JW, Jin M, et al. Phenotypic polarization of activated astrocytes: the critical role of lipocalin-2 in the classical inflammatory activation of astrocytes. Journal of immunology (Baltimore, Md : 1950). 2013; 191: 5204-19.
45. Nam Y, Kim JH, Seo M, Kim JH, Jin M, Jeon S, et al. Lipocalin-2 protein deficiency ameliorates experimental autoimmune encephalomyelitis: the pathogenic role of lipocalin-2 in the central nervous system and peripheral lymphoid tissues. The Journal of biological chemistry. 2014; 289: 16773-89.
46. Saghazadeh A, Rezaei N. The role of timing in the treatment of spinal cord injury. Biomedicine & pharmacotherapy = Biomedecine & pharmacotherapie. 2017; 92: 128-39.

47. Tran AP, Warren PM, Silver J. The Biology of Regeneration Failure and Success After Spinal Cord Injury. Physiological reviews. 2018; 98: 881-917.
48. Zuo X, Liang Z, Zhang J, Wang S, Zheng Q, Ma Y, et al. Photobiomodulation and diffusing optical fiber on spinal cord's impact on nerve cells from normal spinal cord tissue in piglets. Lasers in medical science. 2021.

Figures

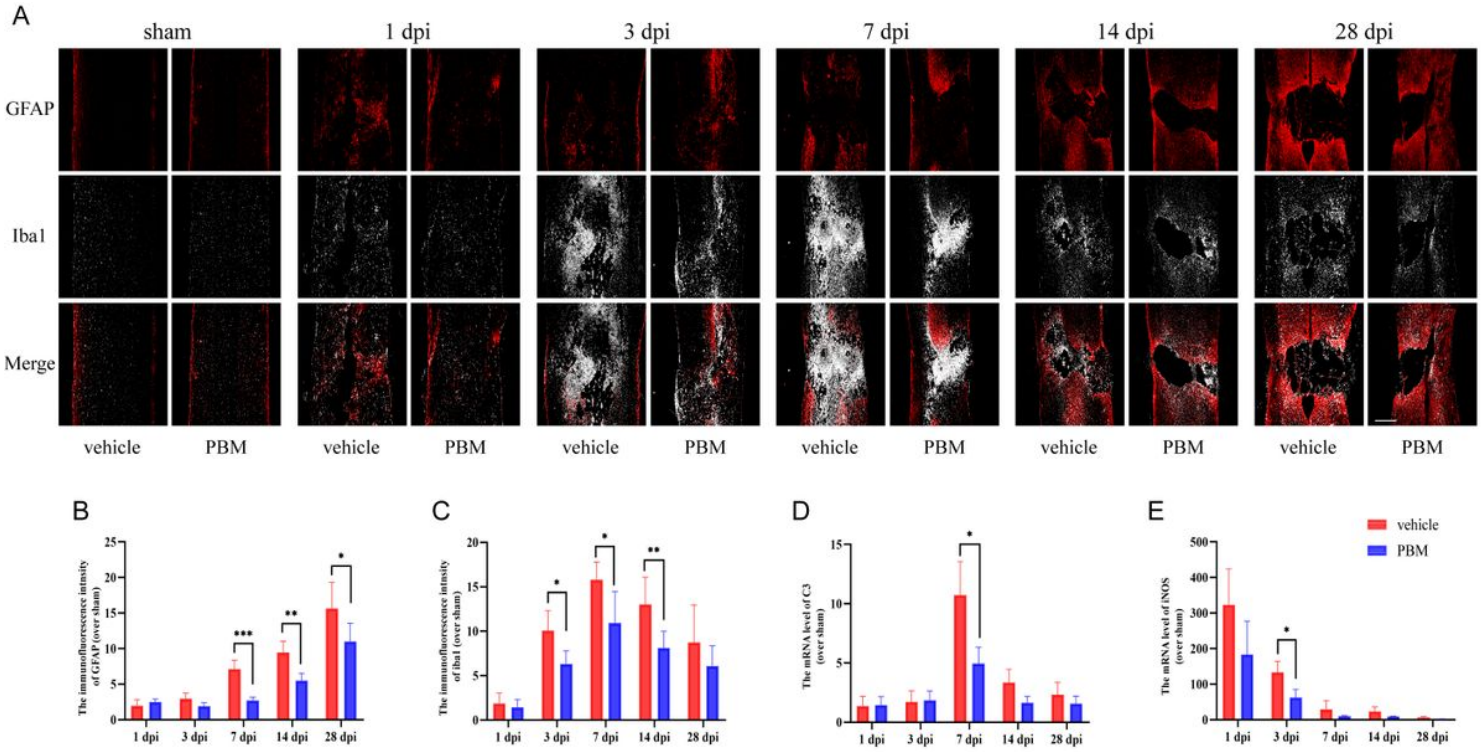

Figure 1

The effect of PBM on the dynamic changes in microglia and astrocytes after SCI. a. Representative images of immunofluorescence staining with GFAP (red) and Iba1 (white) on injured spinal sections in the sham group, vehicle group and PBM group (at 1 dpi, 3 dpi, 7 dpi, 14 dpi and 28 dpi, respectively). b, c. Quantification of the mean fluorescence intensity of GFAP- and Iba1-positive cells. d, e. Relative mRNA expression of C3 and iNOS is presented as the fold change in comparison to the sham group. Scale bar: 400 μm. n=4-6 rats per group. *p < 0.05, **p < 0.01, ***p < 0.001; versus sham group; dpi: days post injury.

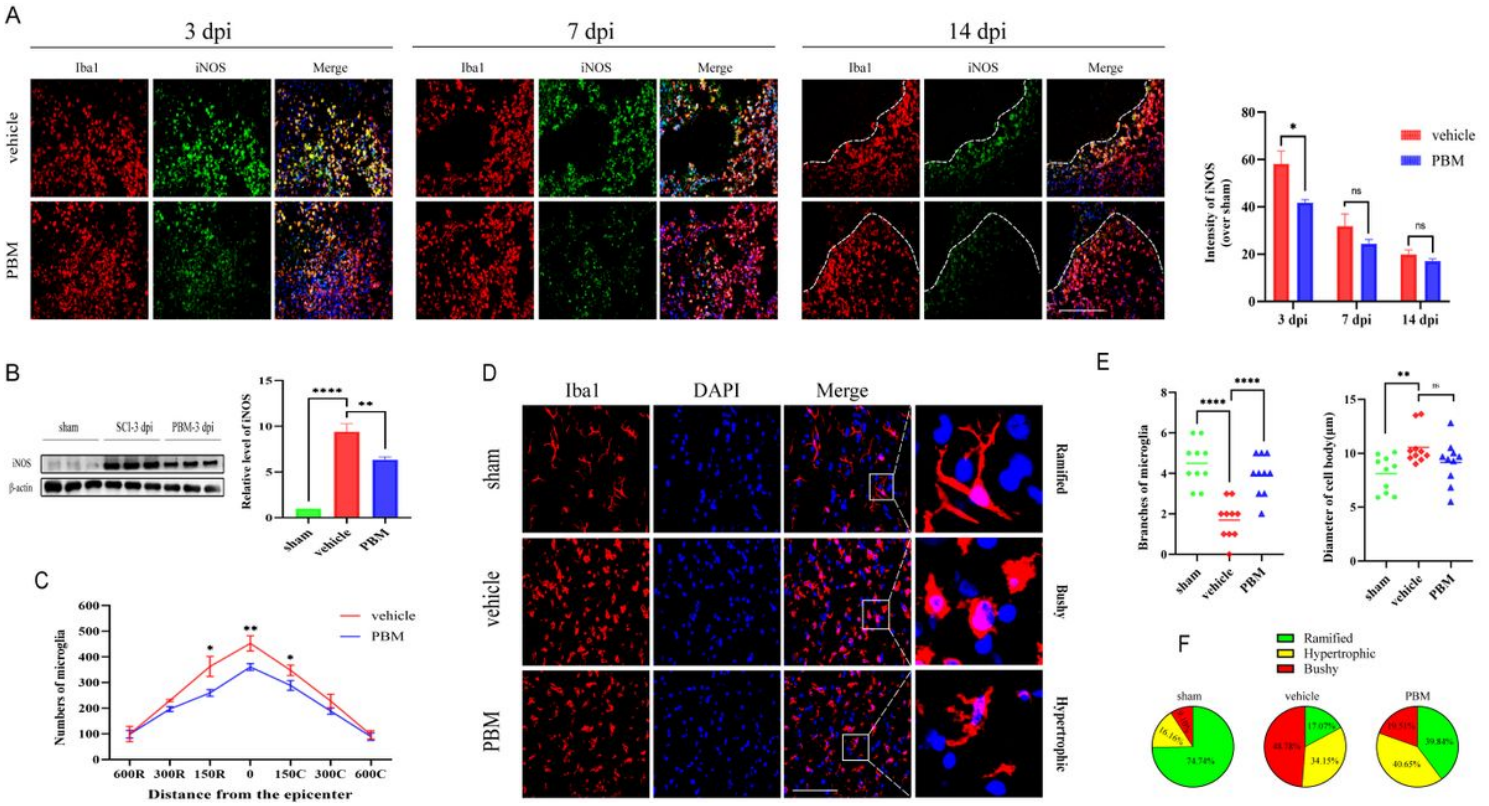

Figure 2

PBM inhibits the activation of neurotoxic microglia after SCI. a. Representative images of immunofluorescence staining with Iba1 (red) and iNOS (green) taken from the lesion area at 3 dpi, 7 dpi, and 14 dpi. Quantification of the intensity of iNOS relative to the sham group. b. Representative blots and quantification showing the expression level of iNOS in the injured spinal cord at 3 dpi. c. Quantification of Iba1-positive cells at different distances to the epicentre from rostral to caudal (600 μm, 300 μm, 150 μm). d. Representative images of microglia 150 μm from the epicentre in the vehicle group, the PBM group and the sham group control. Microglia were classified into ramified, bushy and hypertrophic phenotypes based on cellular morphological features. e. Microglial morphology was assessed by the number of branches per microglia and the diameter of the cell body per microglia (count 10 microglia per rat, n=3 rats per group). f. Quantification of the percentage of ramified, hypertrophic and bushy microglia phenotypes 150 μm from the epicentre in the vehicle group, PBM group, and sham group control. Scale bar: 200 μm, n=3 rats per group. *p <0.05, **p <0.01, ***p <0.001, ****p <0.0001, ns=nonsignificant.

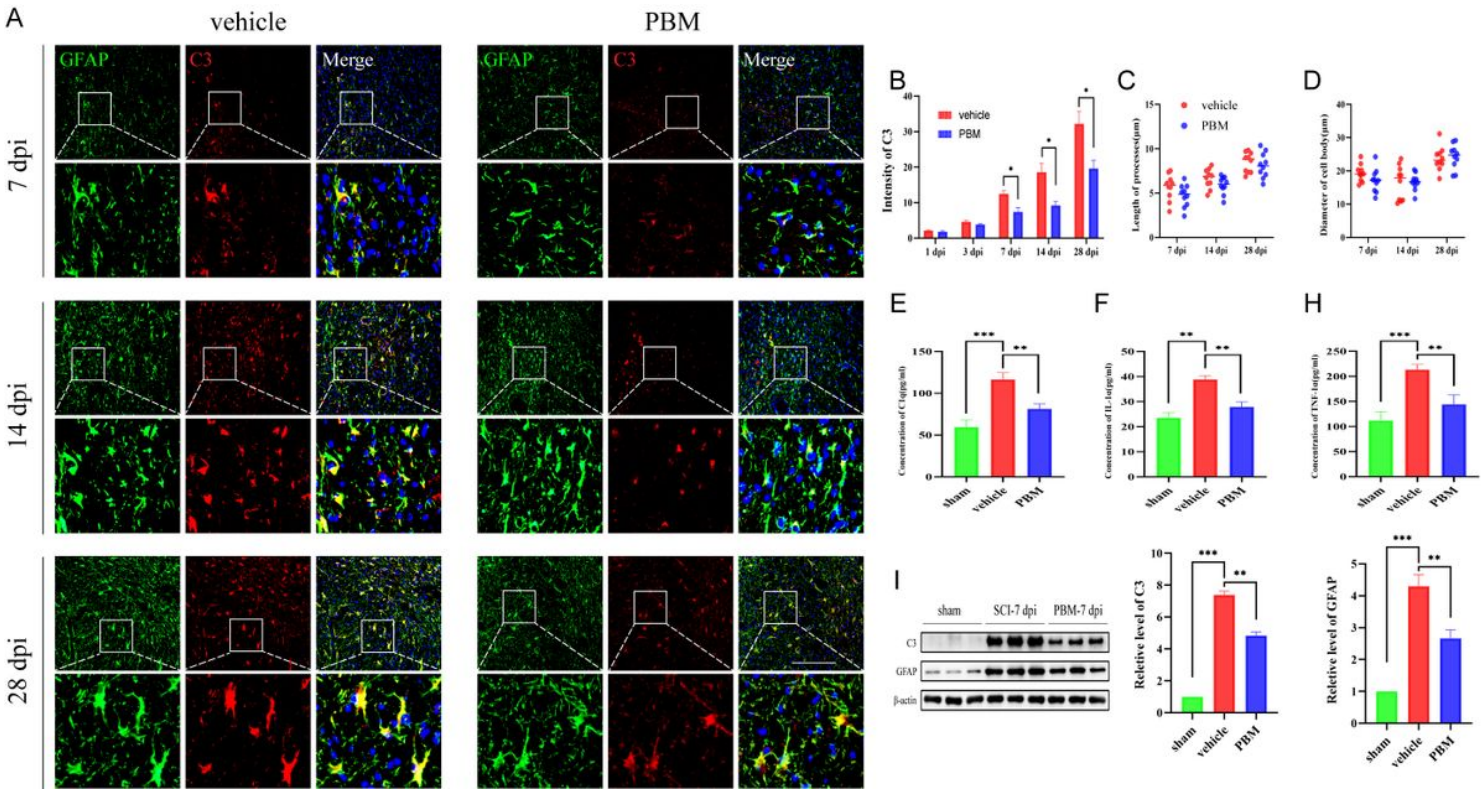

Figure 3

PBM inhibits the activation of A1 astrocytes after SCI. a. Representative images of immunofluorescence staining with GFAP (green) and C3 (red) taken from the lesion area in the vehicle and PBM groups at 7 dpi, 14 dpi and 28 dpi. b. Quantification of the fluorescence intensity of C3 in the vehicle group and PBM group relative to the sham group. c, d. Astrocyte morphology was assessed in terms of the length of processes per microglia and the diameter of the cell body per astrocyte (count 10 cells per rat, n=3 rats per group). e-g. ELISA results for C1q, IL-1α and TNF-α in injured spinal cord sections from the sham, vehicle and PBM groups at 3 dpi. h. Representative blot quantification showing the expression levels of C3 and GFAP in the sham, vehicle and PBM groups at 7 dpi. Scale bar: 200 μm. n=3 rats per group. *p <0.05, **p <0.01, ***p <0.001.

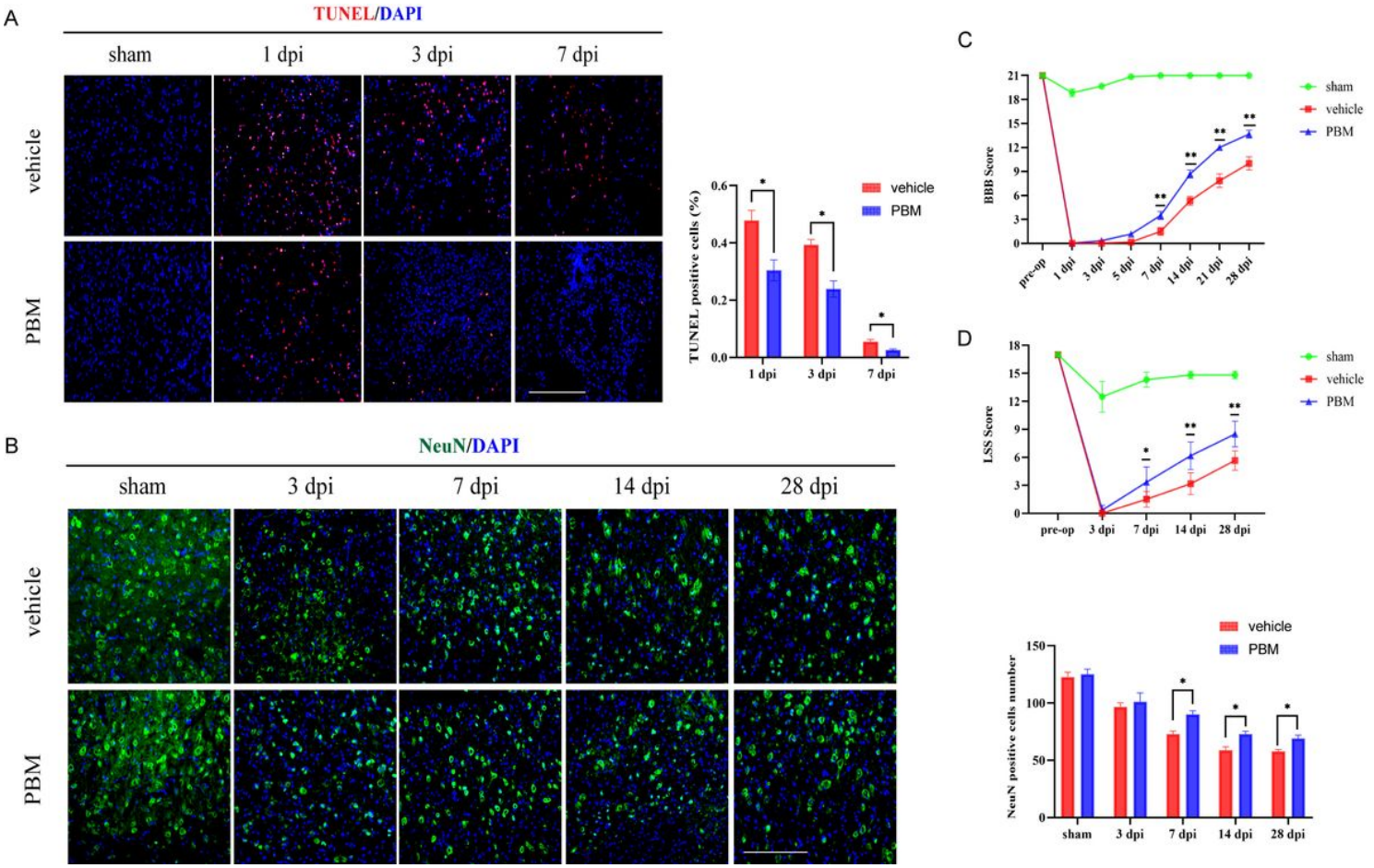

Figure 4

PBM can reduce apoptosis, increase the number of surviving neurons and promote the recovery of motor function after SCI. a. TUNEL staining was used to detect the level of apoptosis at 1 dpi, 3 dpi and 7 dpi. Quantification of apoptotic cells in the spinal dorsal horn in the vehicle and PBM groups. Five visual fields of each sample were randomly selected and analysed (n=3 rats per group). b. The number of surviving neurons in the ventral spinal cord gradually decreased within 28 dpi. Quantification of the number of NeuN-positive cells in the vehicle and PBM groups. Five visual fields of each sample were randomly selected and analysed (n=3 rats per group). c, d. The BBB score and Louisville Swim Scale were used to evaluate the recovery of motor function in the group (n=6 rats per group). *p <0.05, **p <0.01.

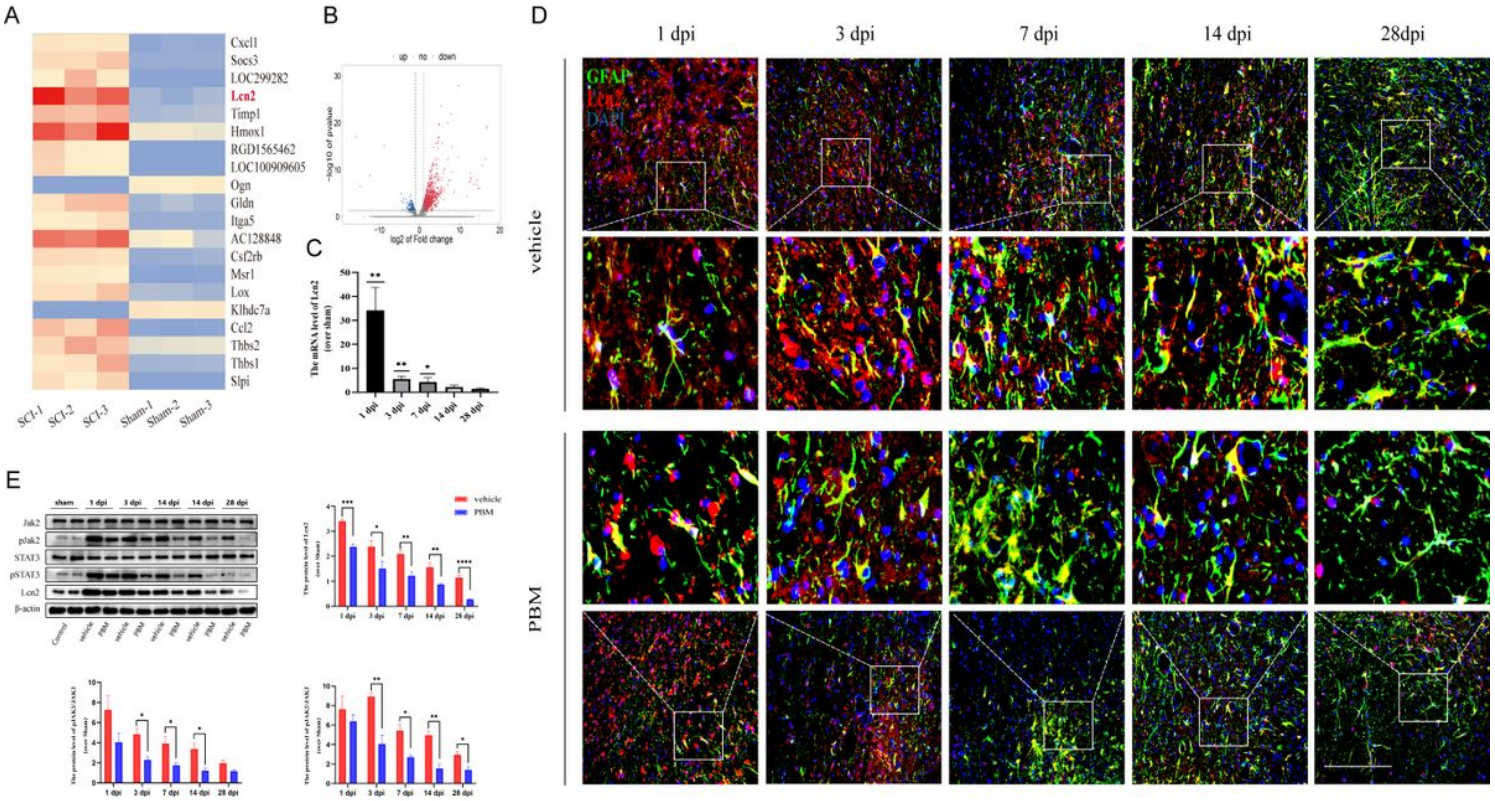

Figure 5

PBM inhibits the secretion of Lcn2 and the activation of the JAK2-STAT3 pathway after SCI. a, b. The 1379 upregulated and 168 downregulated genes in the sham and SCI groups at 1 dpi. The heatmap indicated that Lcn2 was one of the highly upregulated genes. c. The relative mRNA expression of Lcn2 is presented as the fold change in different groups after SCI in comparison to the sham group. d. Representative images of immunofluorescence staining with GFAP (green), C3 (red) and DAPI (blue) taken from the lesion area in the vehicle and PBM groups at 1 dpi, 3 dpi, 7 dpi, 14 dpi and 28 dpi. e. Representative blots showing the expression levels of JAK2, pJAK2, STAT3, pSTAT3 and Lcn2 in the sham, vehicle and PBM groups at 1 dpi, 3 dpi, 7 dpi, 14 dpi and 28 dpi. Quantification of the relative expression of Lcn2, pJAK2/JAK2 and pSTAT3/STAT3. Scale bar: 200 μm, n=3 rats per group. *p <0.05, **p <0.01.

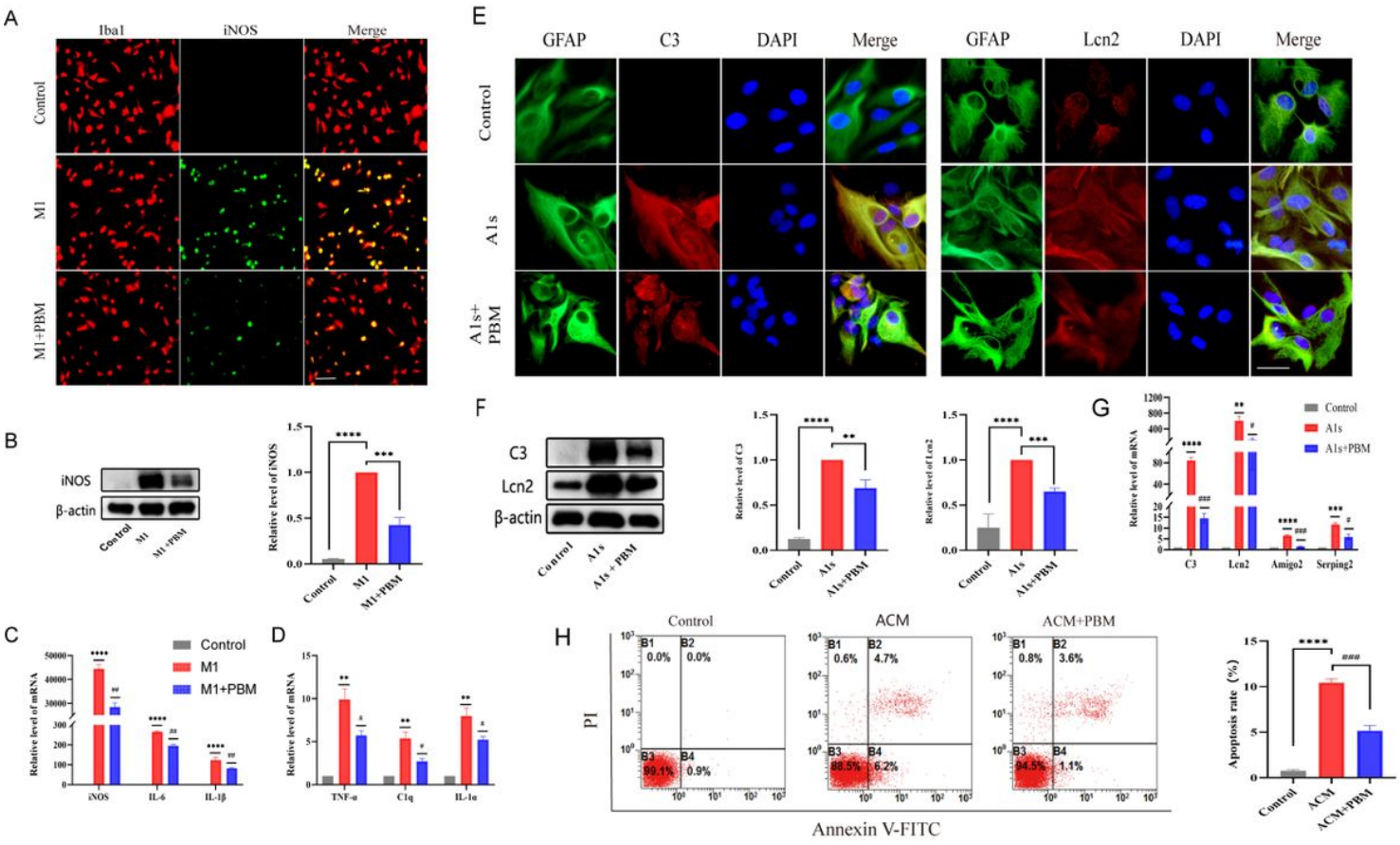

Figure 6

PBM inhibits the activation of M1 microglia and A1 astrocytes in vitro. a. Representative images of immunofluorescence staining with Iba1 (red) and iNOS (green) in the control, M1 and M1+PBM groups. b. Western blotting was used to detect the protein levels of iNOS in the control, M1 and M1+PBM groups. c, d. RT-PCR was used to detect the mRNA levels of iNOS, IL-6, IL-1β, TNF-α, C1q and IL-1α in the control, M1 and M1+PBM groups. e. Representative images of immunofluorescence staining with GFAP (green) and C3 (red) or Lcn2 (red) in the control, A1s and A1s+PBM groups. f. Western blotting was used to detect the protein levels of C3 and Lcn2 in the control, A1s and A1s+PBM groups. g. RT-PCR was used to detect the mRNA levels of C3, Lcn2, Amigo2 and Serping1 in the control, A1s and A1s+PBM groups. h. ACM, but not MCM, induced apoptosis in VSC4.1 cells and was inhibited by PBM. Cell apoptosis was measured by flow cytometry. Scale bar: 200 mm. The experiment was independently repeated at least three times. *p <0.05, **p <0.01, ***p <0.001, ****p <0.0001; #p <0.05, ##p <0.01.

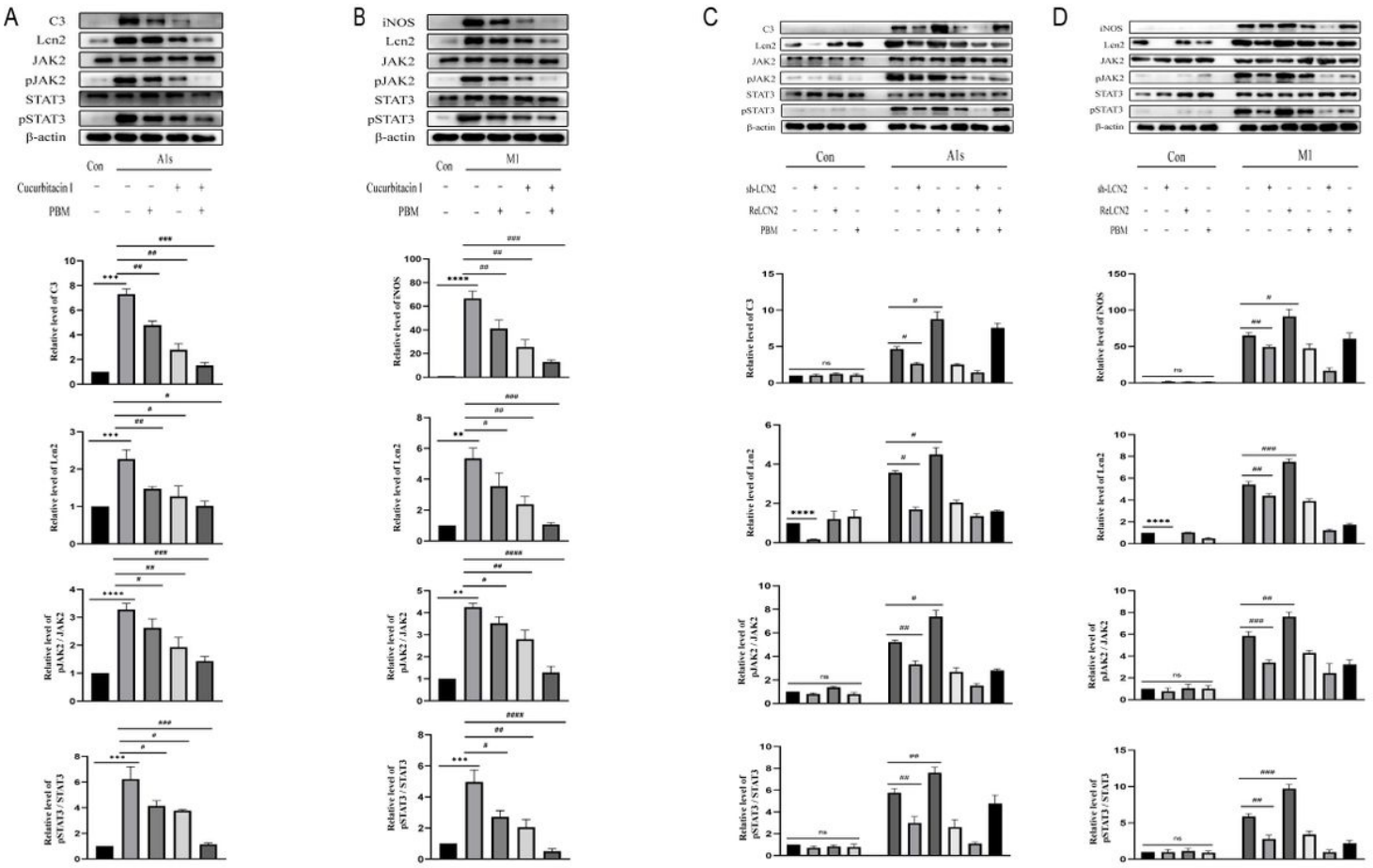

Figure 7

PBM can interfere with the Lcn2/JAK2-STAT3 crosstalk during the activation of neurotoxic glial cells in vitro. PBM and cucurbitacin I synergistically inhibit the activation of astrocytes (a) and microglia (b). Representative blots showing the expression levels of C3 (or iNOS), Lcn2, JAK2, pJAK2, STAT3 and pSTAT3 in different groups. Quantification of the relative levels of C3 (or iNOS), Lcn2, pJAK2/JAK2, and pSTAT3/STAT3. A1 astrocytes (c) and M1 microglia (d) were treated with PBM combined with lentivirus transfection to knock down Lcn2 or additional recombinant Lcn2 protein, respectively. Representative blots showing the expression levels of C3 (or iNOS), Lcn2, JAK2, pJAK2, STAT3 and pSTAT3 in different groups. Quantification of the relative levels of C3 (or iNOS), Lcn2, pJAK2/JAK2, and pSTAT3/STAT3. The experiment was independently repeated at least three times. *p <0.05, **p <0.01, ***p <0.001, ****p <0.0001; #p <0.05, ##p <0.01, ###p <0.001, ####p <0.0001.

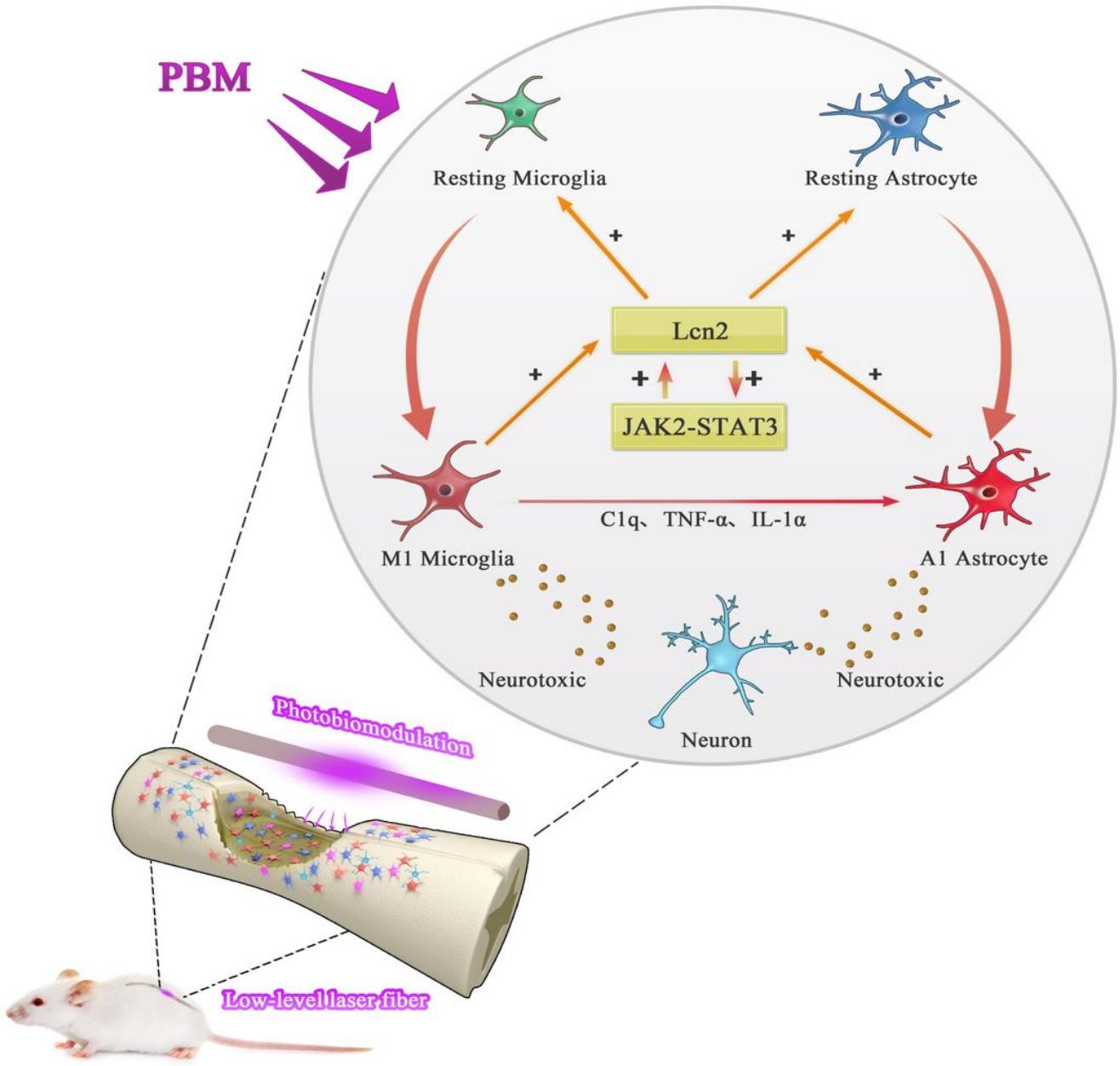

Figure 8

Schematic diagram showing the implantation of a laser fibre in rats after SCI. Resting microglia and astrocytes begin to activate and participate in neuroinflammation after SCI. The activation of A1 astrocytes is induced by the secretion of C1q, TNF-α, and IL-1α from activated microglia, and both M1 microglia and A1 astrocytes are toxic to neurons. The activation of M1 microglia and A1 astrocytes involves Lcn2/JAK2-STAT3 pathway crosstalk: the JAK2-STAT3 pathway contributes to the activation of neurotoxic glial cells and the expression of Lcn2. In turn, Lcn2 exacerbates the activation of M1 microglia and A1 astrocytes and upregulates the activation of the JAK2-STAT3 pathway. The mechanism by which PBM exerts neuroprotection may be related to inhibiting the Lcn2/JAK2-STAT3 crosstalk, which interferes with the activation of M1 microglia and A1 astrocytes.